Geophysical Research Letters

RESEARCH LETTER
10.1029/2025GL119342

Key Points:

- Influences of sampling interval and observation duration on semidiurnal internal tide coherent and incoherent characteristics are examined
- Both the coherent and incoherent characteristics exhibit convergence with increasing observation duration for 1-hr interval
- Coarse satellite sampling yields a larger bias in coherent characteristic, which does not monotonously decrease with increasing duration

Supporting Information:

Supporting Information may be found in the online version of this article.

Correspondence to:

A. Cao,
caoanzhou@zju.edu.cn

Citation:

Cao, A., Guo, Z., Song, J., & Guo, X. (2026). On the coherent and incoherent characteristics of semidiurnal internal tides near the Luzon Strait: Influences of sampling interval and observation duration. *Geophysical Research Letters*, *53*, e2025GL119342. https://doi.org/10.1029/2025GL119342

Received 11 SEP 2025
Accepted 9 FEB 2026

Author Contributions:

Conceptualization: Anzhou Cao
Data curation: Anzhou Cao
Formal analysis: Anzhou Cao, Zheng Guo
Funding acquisition: Anzhou Cao
Investigation: Anzhou Cao
Methodology: Anzhou Cao, Zheng Guo
Supervision: Jinbao Song, Xinyu Guo
Visualization: Anzhou Cao
Writing – original draft: Anzhou Cao, Zheng Guo
Writing – review & editing: Anzhou Cao, Zheng Guo, Jinbao Song, Xinyu Guo

On the Coherent and Incoherent Characteristics of Semidiurnal Internal Tides Near the Luzon Strait: Influences of Sampling Interval and Observation Duration

Anzhou Cao[1], Zheng Guo[2], Jinbao Song[1], and Xinyu Guo[3]

[1]State Key Laboratory of Ocean Sensing & Ocean College, Zhejiang University, Zhoushan, China, [2]Marine Science and Technology College, Zhejiang Ocean University, Zhoushan, China, [3]Center for Marine Environmental Studies, Ehime University, Matsuyama, Japan

Abstract Internal tides (ITs) usually exhibit incoherent characteristics during their propagation. However, estimations of incoherent ITs from different platform (mooring and satellite) observations exhibit discrepancies, partly due to their different sampling intervals and observation durations. Based on 10-year numerical simulation of ITs near the Luzon Strait, we examine influences of sampling interval and observation duration on the coherent and incoherent characteristics of semidiurnal ITs, that is, the M_2 IT steric height and incoherence of semidiurnal ITs in steric height. Results indicate that for 1-hr interval (typical sampling interval of mooring observations), both the coherent and incoherent characteristics of semidiurnal ITs exhibit convergence with increasing duration. However, for 238-hr interval (approximate repeating cycle of TOPEX/Poseidon/Jason-1/Jason-2 satellites), the coherent characteristic of semidiurnal ITs has a larger bias than that for 1-hr interval, and this bias does not monotonously decrease with duration; the semidiurnal IT incoherence has a larger uncertainty than that for 1-hr interval.

Plain Language Summary Internal tides (ITs) are internal waves with tidal frequencies, which can propagate more than 1,000 km away from their source regions. During their long-range propagation, ITs are affected by the varying ocean stratification and subtidal motions. Consequently, ITs gradually lose the phase-locked feature with the astronomic tidal forcing at their source regions, causing incoherent ITs. However, the present estimations of incoherent ITs from different platform (mooring and satellite) observations show some inconsistency, which is speculated to be partly attributed to their different sampling intervals and observation durations. To validate this speculation, we conduct 10-year numerical simulation of ITs near the Luzon Strait. Through re-sampling the simulation results with different intervals, we find that the coarse sampling of satellite observations not only yields a larger bias of the M_2 IT steric height, one coherent characteristic of semidiurnal ITs, but also causes larger uncertainty of semidiurnal IT incoherence in the steric height, compared to the typical sampling interval of mooring observations.

1. Introduction

Internal tides (ITs) are internal waves with tidal frequencies, which are ubiquitous in the global ocean (Buijsman et al., 2016; Müller, 2013; Niwa & Hibiya, 2011, 2014; Simmons et al., 2004; Zhao, 2019). They are typically generated by barotropic tidal currents flowing over rough topographies, such as the mid-ocean ridges, seamounts, island arcs, and continental slopes and shelves. Once generated, ITs can propagate thousands of kilometers away from their source regions (e.g., Zhao, 2014; Zhao et al., 2010). During their long-range propagation, ITs are affected by the varying ocean stratification and subtidal motions such as largescale circulations, mesoscale eddies and jets. Consequently, ITs gradually lose coherence, that is, the phase-locked feature with the astronomic tidal forcing at their source region, and incoherence is increased (Buijsman et al., 2017; Cao et al., 2017, 2022; Egbert & Erofeeva, 2021; Kelly & Lermusiaux, 2016; Kerry et al., 2016; Lahaye et al., 2024; Pickering et al., 2015; Savage et al., 2020; Xu et al., 2013, 2014; Zaron, 2017; Zhao et al., 2010). Because incoherent ITs usually have a larger proportion of high modes than coherent ITs, they can cause stronger vertical shear and contribute more to the turbulent mixing (e.g., Cao et al., 2019; Liu et al., 2016). Hence, understanding the distribution and variation of incoherent ITs is of great importance. Furthermore, incoherent ITs are a significant source of ageostrophic sea level variability for the Surface Water Ocean Topography (SWOT) satellite altimeter mission (Zaron, 2017). Separating them from the balanced

motions remains a big challenge for SWOT observations (Egbert & Erofeeva, 2021; Fu & Ubelmann, 2014; Torres et al., 2019).

Analysis of moored observations through filtering and harmonic analysis is the conventional method to quantify incoherent ITs (e.g., Cao et al., 2017; Eich et al., 2004; Liu et al., 2016; Pickering et al., 2015; van Haren, 2004; Xu et al., 2013, 2014; Zhao et al., 2010). Over the past decade, several methods have been proposed to estimate the IT incoherence from satellite observations (Egbert & Erofeeva, 2021; Zaron, 2017). Based on 23-year combined records of the TOPEX/Poseidon, Jason-1, and Jason-2 satellite altimeter observations, Zaron (2017) used harmonic analysis and along-track wavenumber spectral analysis of sea surface height to estimate the incoherence of semidiurnal ITs (mainly the M_2). Zaron (2017) showed the global map of IT incoherence and revealed that incoherent ITs are stronger than coherent ITs in the majority of equatorial Pacific and Indian Oceans. Aiming to estimate incoherent ITs from SWOT observations, Egbert and Erofeeva (2021) developed an approach that combines harmonic analysis with principal component analysis. Based on this methodology and 1-year HYbrid Coordinate Ocean Model (HYCOM) simulation results, Egbert and Erofeeva (2021) obtained the spatial patterns and temporal variations of the predominant IT constituents on the Amazon Shelf and reproduced the incoherent IT characteristics.

Although various methods have been proposed to estimate the IT incoherence, significant discrepancies persist among the results. For example, the semidiurnal IT incoherence estimated from moored observations is generally on the level of 20%–40% in the South China Sea Basin (e.g., Cao et al., 2017; Xu et al., 2014), whereas that estimated from satellite observations exceeds 60% (Zaron, 2017). We speculate that this discrepancy is partly due to the differences of sampling interval and observation duration between the moored and satellite platforms: Moored observations typically have a 1-hr sampling interval and an observation duration shorter than 1 year, whereas TOPEX/Poseidon/Jason-1/Jason-2 satellite observations employ a 9.9156-day repeat cycle (approximately 238 hr) with the coverage longer than 30 years. To verify our speculation and examine the influences of sampling interval and observation duration (mainly for mooring and TOPEX/Poseidon/Jason-1/Jason-2 satellite observations) on the coherent and incoherent characteristics of ITs, we conduct a 10-year numerical simulation of ITs with the real forcing near the Luzon Strait (LS), which is selected due to its status as one of the most active IT generation regions in the world (Buijsman et al., 2016; Müller, 2013; Niwa & Hibiya, 2011, 2014; Simmons et al., 2004; Zhao, 2019). Observations showed that the baroclinic velocity and vertical displacement at the LS may exceed 2 m/s and 300 m (Alford et al., 2011), and the westward IT energy flux radiated from the LS could reach 40 ± 8 kW/m (Alford et al., 2015). The ITs generated at the LS could propagate over 1,000 km (Zhao, 2014). The presence of energetic mesoscale eddies (Chen et al., 2011) and diverse intrusion patterns of the Kuroshio Current near the LS (Nan et al., 2011) introduce significant variability, leading to significant incoherent ITs in this region (Cao et al., 2017, 2022; Kerry et al., 2016; Pickering et al., 2015; Xu et al., 2013, 2014; Zaron, 2017).

2. Data and Methods

2.1. Model Configurations

The regional ocean modeling system under the framework of Coastal and Regional Ocean COmmunity model (CROCO, version 1.0) was adopted to simulate the ITs near the LS (Figure 1a) from 1 July 2005 to 31 July 2015. The simulated domain (115.5°E–126.5°E and 15.5°N–24.5°N), horizontal resolution (1/20°), sigma layer (30 layers in the vertical direction), sponge layer (0.5° at four open boundaries) and turbulent mixing parameterization schemes were the same as Cao et al. (2023). The barotropic tidal forcing (M_2, S_2, N_2, K_2, K_1, O_1, P_1, Q_1, M_f, and M_m) was obtained from the Oregon State University global model of ocean tides (TPXO7, Egbert & Erofeeva, 2002). The initial and boundary conditions were provided by the HYCOM reanalysis data. The surface forcing was obtained from the Climate Forecast System Reanalysis data. The simulated results were output every 1 hr. To ensure that the simulated ITs have reached a stable state, the simulated results in July 2005 were discarded. Thus, the 10-year numerical simulation results (from August 2005 to July 2015) were used for further analysis. The simulation results reasonably reproduce the ITs and Kuroshio Current patterns near the LS in most of the simulation period (Figures S1 and S2 in Supporting Information S1).

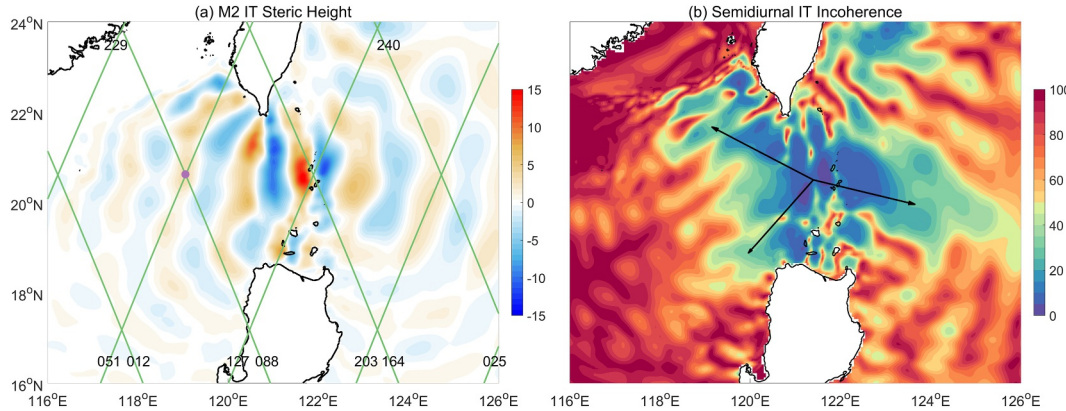

Figure 1. (a) The M_2 internal tide (IT) steric height (shading, unit: cm) near the Luzon Strait (LS). The green lines denote the TOPEX/Poseidon/Jason-1/Jason-2 tracks in the domain. The purple point indicates the crossing point of tracks 051 and 088. (b) Semidiurnal IT incoherence (shading, unit: %) near the LS. The three black quivers indicate the approximate propagation directions of semidiurnal ITs near the LS. Both results shown in panels (a, b) are obtained from 10-year simulation results with 1-hr interval.

2.2. Methodology

As in Egbert and Erofeeva (2021), the steric height (marked as η) was calculated following Savage et al. (2017). Thereafter, harmonic analysis was conducted to calculate the amplitude (H) and phase (g) of semidiurnal ITs (M_2, S_2, N_2, and K_2). The M_2 IT steric height ($\eta_{M2} = H_{M2} \cos g_{M2}$) was used to represent the coherent characteristic of semidiurnal ITs and to assess the influences of sampling interval and observation duration. Considering that the alias synodic periods of each pair of tidal constituents vary with the sampling interval (Fang et al., 2004; Foreman & Henry, 1989), different combinations of sampling interval and observation duration were considered in this study. For 1-hr interval (typical sampling interval of mooring observations), the duration varied from 6 months to 10 years; whereas for 238-hr interval (approximate sampling interval of TOPEX/Poseidon/Jason-1/Jason-2 satellites), the duration varied from 4 to 10 years. For all these durations, the data segments began on 1 August 2005.

To estimate the semidiurnal IT incoherence, different methods were adopted for different sampling intervals. For 1-hr interval, the 4th-order Butterworth bandpass filtering with a cutoff frequency of (1.73, 2.13) cpd was used to isolate the semidiurnal steric height (η_2) from the raw steric height (Cao et al., 2017; Zhao et al., 2010). The hindcast of steric height calculated from the amplitudes and phases of the M_2, S_2, N_2, and K_2 constituents was the coherent semidiurnal steric height (η_{2c}). Subtracting η_{2c} from η_2, the incoherent semidiurnal steric height (η_{2i}) was obtained. Thereafter, the semidiurnal IT incoherence was calculated as

$$\gamma = \frac{\langle \mathrm{Var}(\eta_{2i}) \rangle}{\langle \mathrm{Var}(\eta_2) \rangle} \times 100\% \approx \frac{\langle \mathrm{Var}(\eta_{2i}) \rangle}{\langle \mathrm{Var}(\eta_{2c}) \rangle + \langle \mathrm{Var}(\eta_{2i}) \rangle} \times 100\%, \quad (1)$$

in which Var represents the variance and $< >$ denotes time averaging. For 238-hr interval, the along-track wavenumber spectral method proposed by Zaron (2017) was used. We chose tracks 051 and 088 (Figure 1a) as examples to estimate the semidiurnal IT incoherence in the South China Sea.

3. Results

3.1. Coherent and Incoherent Characteristics for 1-hr Sampling

Figure 1a shows the M_2 IT steric height (η_{M2}) for 10-year simulation results with 1-hr interval. The η_{M2} for other durations is illustrated in Figure S3 in Supporting Information S1. Overall, the η_{M2} extracted from all the durations exhibits a consistent spatial pattern, which closely resembles that of the sea surface height induced by the mode-1 M_2 ITs derived from multiple satellite altimeter observations (Figure S3l in Supporting Information S1, Zhao, 2019), demonstrating the reasonability of simulated ITs again. The η_{M2} is found to be a little larger than that derived from satellite altimeter observations, because higher-mode signals are contained in the simulation results. From the η_{M2}, it is easy to find that the M_2 ITs generated at the LS mainly propagate westward into the South

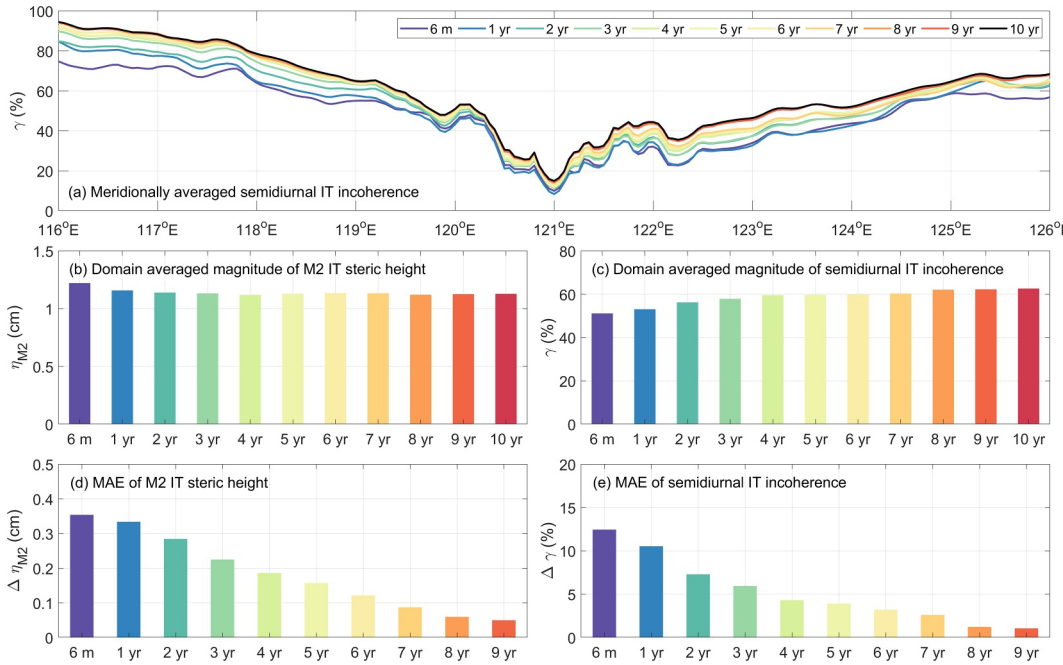

Figure 2. (a) Meridionally averaged semidiurnal internal tide (IT) incoherence as a function of longitude, domain averaged magnitude of (b) the M_2 IT steric height and (c) semidiurnal IT incoherence, and mean absolute errors of (d) the M_2 IT steric height and (e) semidiurnal IT incoherence for simulation results with 1-hr interval.

China Sea and eastward into the Philippine Sea (e.g., Alford et al., 2011; Kerry et al., 2014, 2016; Zhao, 2014, 2019).

Figure 1b displays the semidiurnal IT incoherence (γ) for 10-year simulation results with 1-hr interval. The γ for other durations is illustrated in Figure S4 in Supporting Information S1. Similar to the η_{M2}, the γ extracted from different durations also shares a similar spatial pattern: The incoherence is relatively small near the generation source and along the beams of semidiurnal ITs radiated from the LS; whereas the incoherence generally increases with the distance away from the generation source and IT beams. The γ pattern is generally consistent with previous observations, which gradually increases from the LS to the northwestern continental slope of the South China Sea, and exhibits north-south asymmetry in the South China Sea Basin and east-west asymmetry to either side of the LS (Cao et al., 2017; Lee et al., 2012; Pickering et al., 2015; Xu et al., 2013, 2014). Moreover, low incoherence is found to the east of Taiwan Island, which is attributed to the ITs generated at the I-Lan Ridge.

Although the spatial pattern of η_{M2} (γ) exhibits considerable consistency across different durations, discrepancies persist. As shown in Figure 2a, the meridionally averaged semidiurnal IT incoherence apparently exhibits an increasing trend with duration. This is because longer observation durations increasingly capture the effects of seasonal and interannual variations of ITs (e.g., Zhai et al., 2020; Zhao & Qiu, 2023), which are an important source of IT incoherence (Savage et al., 2020; Zaron & Egbert, 2014). The discrepancy of meridionally averaged incoherence between 6-month and 10-year simulation results is generally on the level of 10%–20%. We also note that with the increase of duration, this discrepancy is gradually reduced. For example, the discrepancy of meridionally averaged incoherence between 9- and 10-year simulation results is nearly invisible. Actually, both the η_{M2} and γ exhibit convergence with increasing duration (Figures 2b and 2c). Hence, the M_2 IT steric height and semidiurnal IT incoherence, derived from 10-year simulation results with 1-hr interval (Figure 1), were used as benchmarks for quantifying the discrepancies caused by different durations, using the mean absolute errors (MAEs) as the evaluation metric:

$$\Delta\eta_{M2} = \frac{1}{N}\sum_{i=1}^{N}\left|\eta_{M2}(i) - \eta_{M2}^{10}(i)\right|, \quad (2)$$

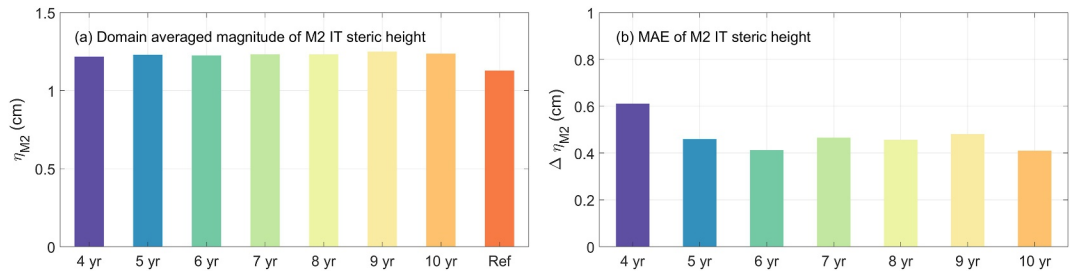

Figure 3. (a) Domain averaged magnitude and (b) mean absolute error of the M_2 internal tide (IT) steric height for simulation results with 238-hr interval. Note that the reference shown in panel (a) is the M_2 IT steric height calculated from 10-year simulation results with 1-hr interval (η_{M2}^{10}).

$$\Delta\gamma = \frac{1}{N}\sum_{i=1}^{N}\left|\gamma(i) - \gamma^{10}(i)\right|, \tag{3}$$

where N denotes the total grid number in the study domain, η_{M2}^{10} and γ^{10} are the M_2 IT steric height and semidiurnal IT incoherence derived from 10-year simulation results with 1-hr interval, respectively, and η_{M2} and γ are those derived from simulation results of other durations.

As shown in Figures 2d and 2e, both $\Delta\eta_{M2}$ and $\Delta\gamma$ are monotonously decreased with duration. These results indicate that both the coherent and incoherent properties of semidiurnal ITs exhibit convergence with increasing duration. Remarkably, extending the duration from 6 months to 9 years can significantly reduce $\Delta\eta_{M2}$ (from 0.35 to 0.05 cm) and $\Delta\gamma$ (from 12.5% to 1.1%) by one order of magnitude. These results suggest that if we have sufficiently long observations with 1-hr interval, we can obtain the accurate coherent and incoherent characteristics of semidiurnal ITs.

3.2. Coherent and Incoherent Characteristics for 238-hr Sampling

We then calculate η_{M2} for simulation results with 238-hr interval and obtain similar spatial patterns as Figure 1a (Figure S5 in Supporting Information S1). However, such η_{M2} has large deviation in the magnitude with that for simulation results with 1-hr interval. Also taking η_{M2}^{10} (Figure 1a) as the reference, we can find that the domain averaged magnitude of η_{M2} for 238-hr interval is apparently larger than η_{M2}^{10} (Figure 3a). At the same time, $\Delta\eta_{M2}$ for 238-hr interval varies from 0.41 to 0.61 cm (Figure 3b), which even exceeds the maximum $\Delta\eta_{M2}$ for 1-hr interval (0.35 cm, Figure 2d). Because η_{M2} is calculated through harmonic analysis, we can conclude that the large $\Delta\eta_{M2}$ for 238-hr interval is attributed to the coarse sampling interval. More importantly, $\Delta\eta_{M2}$ for 238-hr interval exhibits oscillatory behaviors rather than monotonously decreases with duration (Figure 3b). This result suggests that extending the observation duration may not decrease $\Delta\eta_{M2}$ when the sampling interval is 238 hr.

Attention is then paid to the semidiurnal IT incoherence estimated through the spectral method. Figures 4a and 4b show the two-dimensional wavenumber spectra of semidiurnal steric height (η_2) and M_2 IT steric height (η_{M2}) in the South China Sea. They are overall similar, confirming that the M_2 dominates the semidiurnal ITs in the South China Sea. The difference between the two spectra arises from the non-predominant semidiurnal ITs (S_2, N_2, and K_2) and semidiurnal incoherent ITs. Moreover, according to the spectra, the semidiurnal ITs mainly propagate westward and southwestward in the South China Sea, which are consistent with previous simulations (e.g., Cao et al., 2022; Guo et al., 2020; Kerry et al., 2014; Xu et al., 2016).

According to Zaron (2017), the mesoscale sea level anomaly induced by subtidal motions should be first removed before estimating the M_2 IT incoherence. Because our simulations are not totally the same as the real ocean, we cannot directly use satellite-observation-based mesoscale sea level anomaly products (Ray & Byrne, 2010; Ray & Zaron, 2016). Alternatively, we adopted the highpass filtering with a cutoff frequency of 0.5 cpd to the raw simulation results with 1-hr interval to remove the steric height induced by subtidal motions (Figures 4c and 4d as examples). Thereafter, the processed steric height along tracks 051 and 088 was selected every 238 hr.

10.1029/2025GL119342

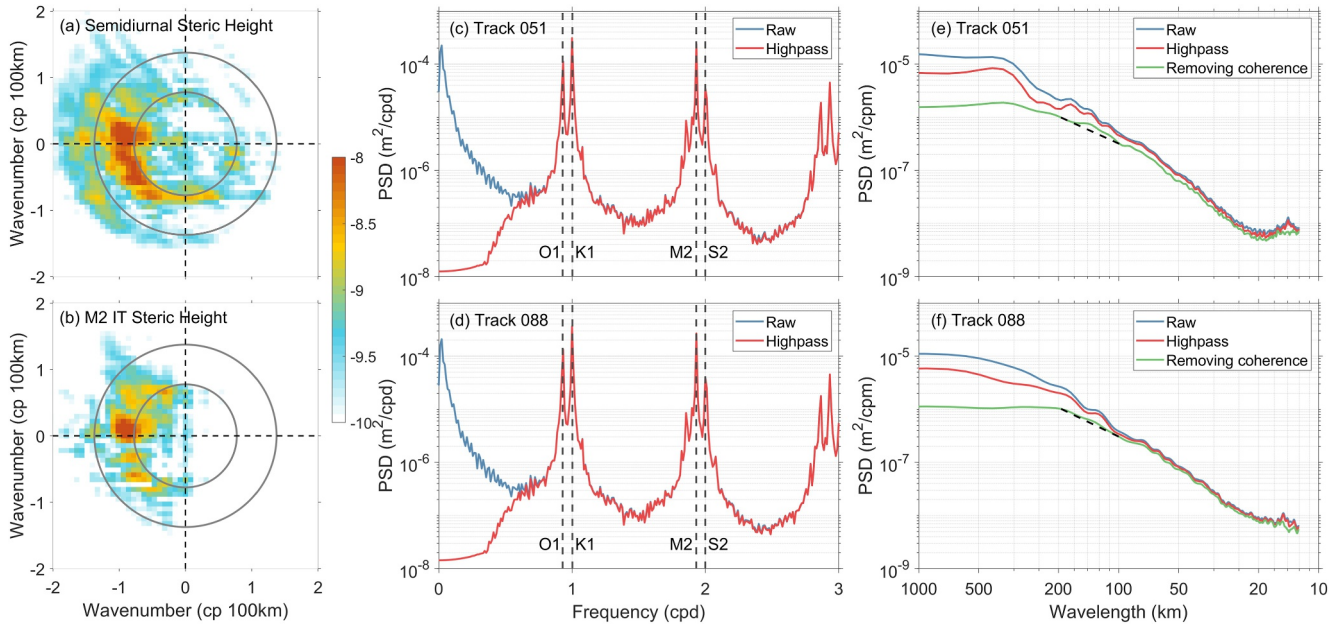

Figure 4. (a) Two-dimensional wavenumber spectrum (shading, in the log form) of semidiurnal steric height (η_2) in August 2005 in the South China Sea. The two gray circles denote the theoretical wavelengths of mode-1 and mode-2 semidiurnal internal tides (ITs). (b) Same as (a) but for the M_2 IT steric height (η_{M2}). Frequency spectra of raw (blue) and highpass filtered steric height (red) near the crossing point (The purple point in Figure 1) of tracks (c) 051 and (d) 088. Vertical dashed lines indicate the predominant diurnal and semidiurnal ITs. Wavenumber spectra of raw (blue) and highpass filtered steric height (red) as well as that removing coherence (green) along tracks (e) 051 and (f) 088. The black dashed line denotes the nontidal broadband, as in Zaron (2017).

Figures 4e and 4f show the wavenumber spectra of raw and highpass filtered steric height as well as that removing coherence, corresponding to the S_0, S_1, and S_r spectra in Zaron (2017), along tracks 051 and 088. The black dashed lines are the nontidal broadband (the S_m spectrum in Zaron (2017)). As shown, after removing the coherence, the spectra of steric height still exist bumps over the nontidal broadband between 100 and 200 km wavelength, which correspond to the signals induced by the semidiurnal incoherent ITs. Based on these spectra, the estimated semidiurnal IT incoherence is 17.2% along track 051 and 9.9% along track 088, both of which are much smaller than those estimated through the conventional method for simulation results with 1-hr interval (Figure S6 in Supporting Information S1).

4. Discussion and Summary

Based on 10-year numerical simulation results of ITs with the real forcing near the LS, we examine the coherent and incoherent characteristics of semidiurnal ITs and explore the influences of sampling intervals and observation durations of mooring and TOPEX/Poseidon/Jason-1/Jason-2 satellite observations on them. The M_2 IT steric height, representing the coherent characteristic of semidiurnal ITs in this study, indicates the propagation and phase of the M_2 ITs radiated from the LS. The semidiurnal IT incoherence exhibits site-dependent features: it is relatively small near the generation source and along the beams of semidiurnal ITs; whereas it is increased with the distance away from the generation source and IT beams.

For 1-hr interval, which is the typical sampling interval of mooring observations, both the coherent and incoherent characteristics of semidiurnal ITs exhibit convergence with increasing observation duration. This result suggests that the accurate coherent and incoherent characteristics of semidiurnal ITs can be obtained from sufficiently long observations with 1-hr interval. For 238-hr interval, which is approximately the repeating cycle of TOPEX/Poseidon/Jason-1/Jason-2 satellites, the M_2 IT steric height shares a similar pattern as that for 1-hr interval. However, the MAE of the M_2 IT steric height is apparently larger than that for 1-hr interval. More importantly, the MAE of the M_2 IT steric height for 238-hr interval exhibits oscillatory behaviors rather than monotonously decreases with the observation duration, suggesting that extending the observation duration may not decrease the MAE in this case. The reason is that compared to the 1-hr sampling, the 238-hr sampling produces much sparser

data records. This sparsity reduces the effective signal information, thereby increasing the influence of noise. Consequently, the 238-hr sampling results in larger errors in the derived M_2 amplitude and phase.

It is important to identify the dominant factor contributing to the MAE of the M_2 IT steric height. According to the definition of the M_2 IT steric height, its MAE can arise from the deviation of amplitude (ΔH), deviation of phase (Δg) or a combination of both, as

$$\begin{aligned}\varepsilon &= (H + \Delta H)\cos(g + \Delta g) - H\cos g \\ &= (H\cos g\cos\Delta g - H\cos g) + \Delta H\cos g\cos\Delta g - H\sin g\sin\Delta g - \Delta H\sin g\sin\Delta g,\end{aligned} \tag{4}$$

in which H and g are the references of the M_2 amplitude and phase calculated from 10-year simulation results with 1-hr interval. Note that the domain averaged absolute value of ε is the MAE of the M_2 IT steric height ($\Delta\eta_{M2}$). Figures S7 and S8 and Table S1 in Supporting Information S1 indicate that for 1-hr interval, ε mainly arises from $\Delta H\cos g\cos\Delta g$ and $-H\sin g\sin\Delta g$ with the latter sharing a more similar pattern as and having a higher correlation coefficient with ε. This suggests that the MAE of the M_2 IT steric height is mainly related to Δg, which is due to the variation in the IT propagation speed. Moreover, both ΔH and Δg are decreased with observation duration, accounting for the convergent $\Delta\eta_{M2}$ for 1-hr interval (Figure 2d). However, the situation is different for 238-hr interval. As shown in Figures S9 and S10 in Supporting Information S1, ε also arises from $\Delta H\cos g\cos\Delta g$ and $-H\sin g\sin\Delta g$ but exhibits a different pattern from them. Meanwhile, the correlation coefficient between ε and $\Delta H\cos g\cos\Delta g$ is nearly comparable to that between ε and $-H\sin g\sin\Delta g$ (Table S2 in Supporting Information S1). Moreover, either ΔH or Δg is not significantly decreased with observation duration. Comparing to the error analysis for 1-hr interval, we believe it is the coarse sampling of 238 hr that causes systemic biases in the M_2 amplitude and phase, which finally result in the large MAE of the M_2 IT steric height (Figure 3b).

We also test the influences of sampling intervals (17.0505, 21, and 35 days) of Geosat Follow-On, SWOT and European Remote Sensing Satellite (ERS) on the M_2 IT steric height (Figure S11 in Supporting Information S1), which are similar to that of 238-hr interval. Furthermore, the MAE of the M_2 IT steric height for a certain duration is found to be generally increased with sampling interval, which further confirms that the coarser sampling interval yields worse estimation of IT coherent characteristics. This is generally consistent with the finding of Zhao (2024) that the global mode-1 M_2 ITs extracted from SWOT have large errors. This, on the other hand, indicates that using multiple satellite altimeter observations (e.g., Zhao, 2019) can increase the accuracy of extracted IT coherent characteristics, as it decreases the sampling interval to some extent.

The semidiurnal IT incoherence estimated through the spectral method in this study (~10%) is much smaller than that (>60%) in Zaron (2017) in the South China Sea. This discrepancy arises from several causes. First, Zaron (2017) used satellite-observation-based products (Ray & Byrne, 2010; Ray & Zaron, 2016) to remove the mesoscale sea level anomaly, whereas we adopt highpass filtering to remove it, as our simulations are not totally the same as the real ocean. Second, Zaron (2017) calculated the wavenumber spectrum based on 2,000-km-segment sea surface height data, whereas the segment length used in this study is smaller than 1,000 km due to the simulated domain (Figure 1a). Third, the integration bandwidths of wavenumber spectrum between this study and Zaron (2017) may also differ. However, either our estimation or Zaron (2017)'s estimation deviates from the observed (e.g., Cao et al., 2017; Xu et al., 2014) and simulated semidiurnal IT incoherence (Figure S6 in Supporting Information S1) in the South China Sea to some extent. We believe that the spectral method is an important method to estimate the IT incoherence from satellite observations with coarse sampling interval. However, we should be more cautious when we directly use the IT incoherence estimated through the spectral method.

This study investigates the coherent and incoherent characteristics of semidiurnal ITs near the LS using long-term simulation data. Compared to the traditional mooring- and satellite-observation-based approaches, this method has distinct advantages. It avoids the substantial costs of deploying and retrieving moorings, despite requiring considerable computational resources. It provides more comprehensive results than satellite observations, thereby enabling a quantitative assessment of the coherent and incoherent characteristics of ITs extracted from satellite observations with specific sampling intervals. Moreover, this method can be expanded to other regions as well as the global ocean. At the same time, we acknowledge that this study relies on the numerical simulation. Although our simulations are based on the well-established CROCO and validated against observational data, they remain

approximations and cannot fully replicate the complexity of the real ocean. Nevertheless, the dynamics responsible for incoherent ITs are represented in the simulation framework. Therefore, analyzing these simulation data remains valid for investigating the causal mechanisms. In the future, we plan to develop a machine-learning model trained on these simulation data to establish a quantitative linkage between the raw steric height and its component associated with incoherent ITs. Ultimately, this model will be adapted to process SWOT observations, enabling the isolation of sea surface height signal attributable to incoherent ITs.

Conflict of Interest

The authors declare no conflicts of interest relevant to this study.

Data Availability Statement

The data shown in the figures of this study are available at Cao (2025). The code of CROCO is available at https://www.croco-ocean.org/download/. The HYCOM reanalysis data are downloaded from https://apdrc.soest.hawaii.edu/erddap/griddap/hawaii_soest_2d95_7b3d_ec92.html and https://apdrc.soest.hawaii.edu/erddap/griddap/hawaii_soest_7e38_7a7b_afe2.html. The Climate Forecast System Reanalysis data are downloaded from https://tds.hycom.org/thredds/catalog/datasets/force/ncep_cfsr/netcdf/catalog.html for wind speed at 10 m height (with postfix of uv-10m.nc) from 2005 to 2010 and from https://tds.hycom.org/thredds/catalog/datasets/force/ncep_cfsv2/netcdf/catalog.html for wind speed at 10 m height (with postfix of uv-10m.nc) from 2011 to 2015.

Acknowledgments
This study is partially supported by the National Natural Science Foundation of China (Grant 42176002 and 41806012) and the Fundamental Research Funds for the Central Universities (Grant 226-2025-00150). Anzhou Cao acknowledges the Funding of ZJU Tang Scholar. This study is also supported by the Ministry of Education, Culture, Sports, Science and Technology, Japan (MEXT) to a project on Joint Usage/Research Center–Leading Academia in Marine and Environment Pollution Research (Lamer). The authors also thank Dr. Shuya Wang of Tohoku University for constructive discussions and two anonymous reviewers for valuable suggestions which greatly improve the manuscript.

References

Alford, M. H., MacKinnon, J. A., Nash, J. D., Simmons, H., Pickering, A., Klymak, J. M., et al. (2011). Energy flux and dissipation in Luzon Strait: Two tales of two ridges. *Journal of Physical Oceanography*, *41*(11), 2211–2222. https://doi.org/10.1175/JPO-D-11-073.1

Alford, M. H., Peacock, T., MacKinnon, J. A., Nash, J. D., Buijsman, M. C., Centurioni, L. R., et al. (2015). The formation and fate of internal waves in the South China Sea. *Nature*, *521*(7550), 65–69. https://doi.org/10.1038/nature14399

Buijsman, M. C., Ansong, J. K., Arbic, B. K., Richman, J. G., Shriver, J. F., Timko, P. G., et al. (2016). Impact of parameterized internal wave drag on the semidiurnal energy balance in a global ocean circulation model. *Journal of Physical Oceanography*, *46*(5), 1399–1419. https://doi.org/10.1175/JPO-D-15-0074.1

Buijsman, M. C., Arbic, B. K., Richman, J. G., Shriver, J. F., Wallcraft, A. J., & Zamudio, L. (2017). Semidiurnal internal tide incoherence in the equatorial Pacific. *Journal of Geophysical Research: Oceans*, *122*(7), 5286–5305. https://doi.org/10.1002/2016JC012590

Cao, A. (2025). Data for manuscript 20250908 [Dataset]. *Zenodo*. Retrieved from https://zenodo.org/records/17686392

Cao, A., Guo, Z., Lv, X., Song, J., & Zhang, J. (2017). Coherent and incoherent features, seasonal behaviors and spatial variations of internal tides in the northern South China Sea. *Journal of Marine Systems*, *172*, 75–83. https://doi.org/10.1016/j.jmarsys.2017.03.005

Cao, A., Guo, Z., Wang, S., Chen, X., Lv, X., & Song, J. (2019). Upper ocean shear in the northern South China Sea. *Journal of Oceanography*, *75*(6), 525–539. https://doi.org/10.1007/s10872-019-00520-x

Cao, A., Guo, Z., Wang, S., Chen, X., Song, J., & Guo, X. (2023). Energetics of the M_2 internal tides modulated by typhoons at the Luzon Strait. *Ocean Modelling*, *186*, 102243. https://doi.org/10.1016/j.ocemod.2023.102243

Cao, A., Guo, Z., Wang, S., Guo, X., & Song, J. (2022). Incoherence of the M_2 and K_1 internal tides radiated from the Luzon Strait under the influence of looping and leaping Kuroshio. *Progress in Oceanography*, *206*, 102850. https://doi.org/10.1016/j.pocean.2022.102850

Chen, G., Hou, Y., & Chu, X. (2011). Mesoscale eddies in the South China Sea: Mean properties, spatiotemporal variability, and impact on thermohaline structure. *Journal of Geophysical Research*, *116*(C6), C06018. https://doi.org/10.1029/2010JC006716

Egbert, G. D., & Erofeeva, S. Y. (2002). Efficient inverse modeling of barotropic ocean tides. *Journal of Atmospheric and Oceanic Technology*, *19*(2), 183–204. https://doi.org/10.1175/1520-0426(2002)019<0183:EIMOBO>2.0.CO;2

Egbert, G. D., & Erofeeva, S. Y. (2021). An approach to empirical mapping of incoherent internal tides with altimetry data. *Geophysical Research Letters*, *48*(24), e2021GL095863. https://doi.org/10.1029/2021GL095863

Eich, M. L., Merrifield, M. A., & Alford, M. H. (2004). Structure and variability of semidiurnal internal tides in Mamala Bay, Hawaii. *Journal of Geophysical Research*, *109*(C5), C05010. https://doi.org/10.1029/2003JC002049

Fang, G., Wang, Y., Wei, Z., Choi, B. H., Wang, X., & Wang, J. (2004). Empirical cotidal charts of the Bohai, Yellow, and East China Seas from 10 years of TOPEX/Poseidon altimetry. *Journal of Geophysical Research*, *109*(C11), C11006. https://doi.org/10.1029/2004JC002484

Foreman, M. G. G., & Henry, R. F. (1989). The harmonic analysis of tidal model time series. *Advances in Water Resources*, *12*(3), 109–120. https://doi.org/10.1016/0309-1708(89)90017-1

Fu, L.-L., & Ubelmann, C. (2014). On the transition from profile altimeter to swath altimeter for observing global ocean surface topography. *Journal of Atmospheric and Oceanic Technology*, *31*(2), 560–568. https://doi.org/10.1175/JTECH-D-13-00109.1

Guo, Z., Cao, A., Lv, X., & Song, J. (2020). Impact of multiple tidal forcing on the simulation of the M_2 internal tides in the northern South China Sea. *Ocean Dynamics*, *70*(2), 187–198. https://doi.org/10.1007/s10236-019-01324-9

Kelly, S. M., & Lermusiaux, P. F. J. (2016). Internal-tide interactions with the Gulf Stream and middle Atlantic bight shelfbreak front. *Journal of Geophysical Research: Oceans*, *121*(8), 6271–6294. https://doi.org/10.1002/2016JC011639

Kerry, C. G., Powell, B. S., & Carter, G. S. (2014). The impact of subtidal circulation on internal tide generation and propagation in the Philippine Sea. *Journal of Physical Oceanography*, *44*(5), 1386–1405. https://doi.org/10.1175/JPO-D-13-0142.1

Kerry, C. G., Powell, B. S., & Carter, G. S. (2016). Quantifying the incoherent M_2 internal tide in the Philippine Sea. *Journal of Physical Oceanography*, *46*(8), 2483–2491. https://doi.org/10.1175/JPO-D-16-0023.1

Lahaye, N., Ponte, A., Le Sommer, J., & Albert, A. (2024). Internal tide surface signature and incoherence in the North Atlantic. *Geophysical Research Letters*, *51*(12), e2024GL108508. https://doi.org/10.1029/2024GL108508

Lee, I.-H., Wang, Y.-H., Yang, Y., & Wang, D.-P. (2012). Temporal variability of internal tides in the northeast South China Sea. *Journal of Geophysical Research*, *117*, C02013. https://doi.org/10.1029/2011JC007518

Liu, Q., Xie, X., Shang, X., & Chen, G. (2016). Coherent and incoherent internal tides in the southern South China Sea. *Chinese Journal of Oceanology and Limnology*, *34*(6), 1374–1382. https://doi.org/10.1007/s00343-016-5171-5

Müller, M. (2013). On the space- and time-dependence of barotropic-to-baroclinic tidal energy conversion. *Ocean Modelling*, *72*, 242–252. https://doi.org/10.1016/j.ocemod.2013.09.007

Nan, F., Xue, H., Chai, F., Shi, L., Shi, M., & Guo, P. (2011). Identification of different types of Kuroshio intrusion into the South China Sea. *Ocean Dynamics*, *61*(9), 1291–1304. https://doi.org/10.1007/s10236-011-0426-3

Niwa, Y., & Hibiya, T. (2011). Estimation of baroclinic tide energy available for deep ocean mixing based on three-dimensional global numerical simulations. *Journal of Oceanography*, *67*(4), 493–502. https://doi.org/10.1007/s10872-011-0052-1

Niwa, Y., & Hibiya, T. (2014). Generation of baroclinic tide energy in a global three-dimensional numerical model with different spatial grid resolutions. *Ocean Modelling*, *80*, 59–73. https://doi.org/10.1016/j.ocemod.2014.05.003

Pickering, A., Alford, M., Nash, J., Rainville, L., Buijsman, M., Ko, D. S., & Lim, B. (2015). Structure and variability of internal tides in Luzon Strait. *Journal of Physical Oceanography*, *45*(6), 1574–1594. https://doi.org/10.1175/JPO-D-14-0250.1

Ray, R. D., & Byrne, D. A. (2010). Bottom pressure tides along a line in the southeast Atlantic Ocean and comparisons with satellite altimetry. *Ocean Dynamics*, *60*(5), 1167–1176. https://doi.org/10.1007/s10236-010-0316-0

Ray, R. D., & Zaron, E. D. (2016). M_2 internal tides and their observed wavenumber spectra from satellite altimetry. *Journal of Physical Oceanography*, *46*(1), 3–22. https://doi.org/10.1175/jpo-d-15-0065.1

Savage, A. C., Arbic, B. K., Richman, J. G., Shriver, J. F., Alford, M. H., Buijsman, M. C., et al. (2017). Frequency content of sea surface height variability from internal gravity waves to mesoscale eddies. *Journal of Geophysical Research: Oceans*, *122*(3), 2519–2538. https://doi.org/10.1002/2016JC012331

Savage, A. C., Waterhouse, A. F., & Kelly, S. M. (2020). Internal tide nonstationarity and wave-mesoscale interactions in the Tasman Sea. *Journal of Physical Oceanography*, *50*(10), 2931–2951. https://doi.org/10.1175/JPO-D-19-0283.1

Simmons, H. L., Hallberg, R. W., & Arbic, B. K. (2004). Internal wave generation in a global baroclinic tide model. *Deep-Sea Research II*, *51*(25–26), 3043–3068. https://doi.org/10.1016/j.dsr2.2004.09.015

Torres, H. S., Klein, P., Siegelman, L., Qiu, B., Chen, S., Ubelmann, C., et al. (2019). Diagnosing ocean-wave-turbulence interactions from space. *Geophysical Research Letters*, *46*(15), 8933–8942. https://doi.org/10.1029/2019GL083675

van Haren, H. (2004). Incoherent internal tidal currents in the deep ocean. *Ocean Dynamics*, *54*(1), 66–76. https://doi.org/10.1007/s10236-003-0083-2

Xu, Z., Liu, K., Yin, B., Zhao, Z., Wang, Y., & Li, Q. (2016). Long-range propagation and associated variability of internal tides in the South China Sea. *Journal of Geophysical Research: Oceans*, *121*(11), 8268–8286. https://doi.org/10.1002/2016JC012105

Xu, Z., Yin, B., Hou, Y., & Liu, A. K. (2014). Seasonal variability and north-south asymmetry of internal tides in the deep basin west of the Luzon Strait. *Journal of Marine Systems*, *134*, 101–112. https://doi.org/10.1016/j.jmarsys.2014.03.002

Xu, Z., Yin, B., Hou, Y., & Xu, Y. (2013). Variability of internal tides and near-inertial waves on the continental slope of the northwestern South China Sea. *Journal of Geophysical Research: Oceans*, *118*(1), 197–211. https://doi.org/10.1029/2012JC008212

Zaron, E. D. (2017). Mapping the nonstationary internal tide with satellite altimetry. *Journal of Geophysical Research: Oceans*, *122*(1), 539–554. https://doi.org/10.1002/2016JC012487

Zaron, E. D., & Egbert, G. D. (2014). Time-variable refraction of the internal tide at the Hawaiian Ridge. *Journal of Physical Oceanography*, *44*(2), 538–557. https://doi.org/10.1175/JPO-D-12-0238.1

Zhai, R.-W., Chen, G.-Y., Liang, C.-R., Shang, X.-D., & Xie, J.-S. (2020). The influence of ENSO on the structure of internal tides in the Xisha area. *Journal of Geophysical Research: Oceans*, *125*(3), e2019JC015405. https://doi.org/10.1029/2019JC015405

Zhao, Z. (2014). Internal tide radiation from the Luzon Strait. *Journal of Geophysical Research: Oceans*, *119*(8), 5434–5448. https://doi.org/10.1002/2014JC010014

Zhao, Z. (2019). Mapping internal tides from satellite altimetry without blind directions. *Journal of Geophysical Research: Oceans*, *124*(12), 8605–8625. https://doi.org/10.1029/2019JC015507

Zhao, Z. (2024). Internal tides from SWOT: A 75-day instantaneous mode-1 M_2 internal tide model. *Journal of Geophysical Research: Oceans*, *129*(12), e2024JC021174. https://doi.org/10.1029/2024JC021174

Zhao, Z., Alford, M. H., MacKinnon, J. A., & Pinkel, R. (2010). Long-range propagation of the semidiurnal internal tide from the Hawaiian Ridge. *Journal of Physical Oceanography*, *40*(4), 713–736. https://doi.org/10.1175/2009JPO4207.1

Zhao, Z., & Qiu, B. (2023). Seasonal west-east seesaw of M_2 internal tides from the Luzon Strait. *Journal of Geophysical Research: Oceans*, *128*(3), e2022JC019281. https://doi.org/10.1029/2022JC019281